Synchrotron Rocking Curve X-ray Topography Characterization of High Energy Implanted 4H-SiC Lattice Damage

Zeyu Chen, Hongyu Peng, Yafei Liu , Qianyu Cheng, Shanshan Hu, Balaji Raghothamachar, Michael Dudley
Department of Materials Science and Engineering, Stony Brook University, Stony Brook, NY, USA
Reza Ghandi, Stacey Kennerly
GE Research, Niskayuna, NY, 12309, USA
Peter Thieberger
Brookhaven National Laboratory(BNL), Upton, NY 11973 USA

Stony Brook University
Advanced Photon Source
Argonne National Laboratory

4H-SiC Superjunction Device

Superjunction SiC power device:
- Deep junction
- High breakdown voltage
- Low on-resistance
- High efficiency

Application:
- Hybrid Aircraft:
- High Speed Train:
- Power Grid:
- Shipboard Power System:

Motivation

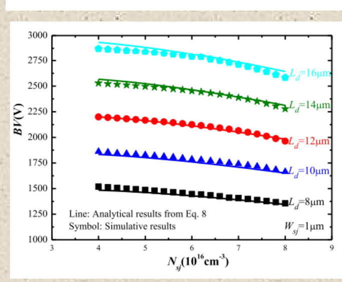

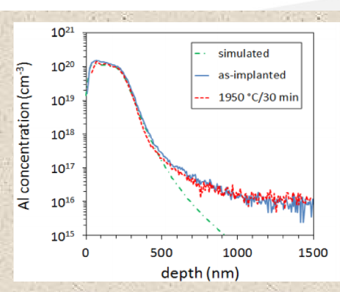

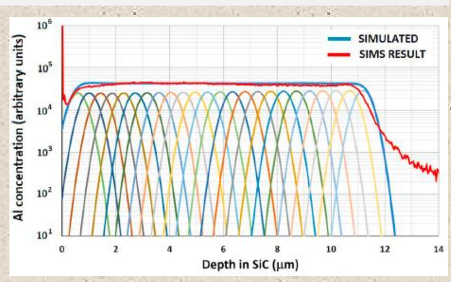

- Energy level of few hundreds keVs are used in conventional ion implantation
- The depth of conventional implantation is usually within 1 um. [2]
- High break down voltage of superjunction SiC device could be realized by thicker drift layer. [1]
- Selective doping would be challenging for thick epilayer.
- More than 10 um of depth could be achieved by high energy ion implantation[3]

Synchrotron X-ray Rocking Curve Topography (SXRCT)

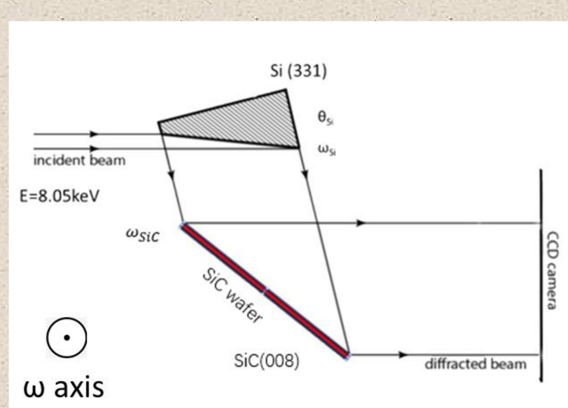

- A beam conditioner (Si(331)) is used with d-spacing close to (0008) d-spacing in SiC to maximize angular resolution
- The crystal sample will only diffract when the Bragg condition is satisfied
- only part of the crystal will diffract due to the lattice distortion inside the crystal
- To image the whole sample, a small angle of rotation about ω axis is applied

$$\frac{\partial u_i}{\partial x_i} = \frac{\omega^{x_i(x_j)} + \omega^{-x_i(x_j)}}{2 \tan \theta_B} \quad (1)$$

$$\frac{\partial u_i}{\partial x_k} = \frac{\omega^{x_i(x_j)} - \omega^{-x_i(x_j)}}{2} \quad (2)$$

- Equation (1) and (2) are used to deconvolute the strain and tile
- $\omega^{x_i(x_j)}$ means that the deviation is from rotating the diffraction plane x_i about x_j axis and θ_B is the perfect Bragg angle for the crystal. $\frac{\partial u_i}{\partial x_i}$ and $\frac{\partial u_i}{\partial x_k}$ are the terms of local lattice dilation/compression and shear/rotation.

Ion Implantation

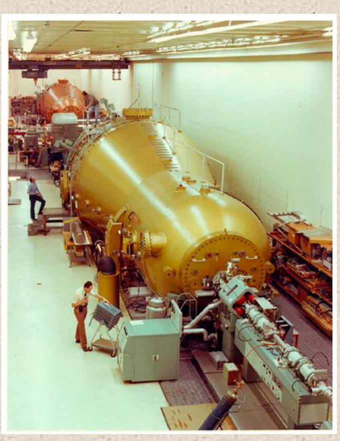

- High energy ion implantation were carried out at the Tandem Van de Graaff facility at Brookhaven National Laboratory[3]
- Samples were implanted with Al or N with energy ranging from 13 MeV to 65.7 MeV. total fluence is 5.56 x 10^{13} cm^{-2} and concentration is 4 x 10^{16} cm^{-3}
- During ion implantation, SiC atoms will be displaced by incoming accelerated ions, so lattice strain will be introduced.

Characterization of As-implanted Sample

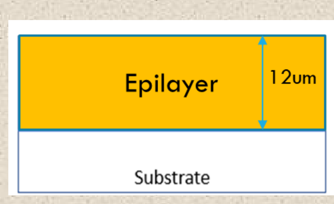

Blanket

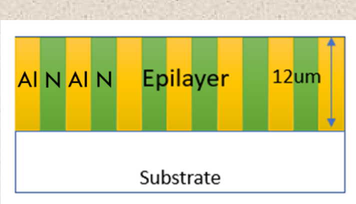

Alternate Al/N Pillar

Sample	Dopant & concentration	Implantation energy (max)	Comments
1	unimplanted	-	-
2	N, 4.4 e 16	42.99MeV	Blanket
3	Al, 4.4e16	65.7MeV	Blanket
4	Al & N, 4.4e16	65.7MeV	Al and N Blanket & Al and N Pillar

- Sample 2 and 3 were implanted with Al or N in blanket pattern
- Sample 4 were implanted with Al/N pillar and co-implanted with Al & N in blanket pattern

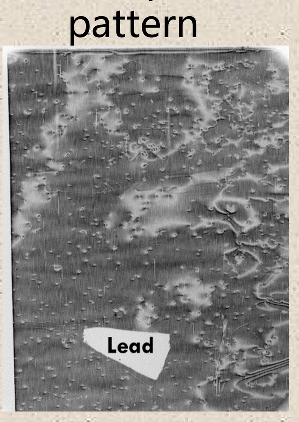

Topograph of sample 1

Topograph of sample 2

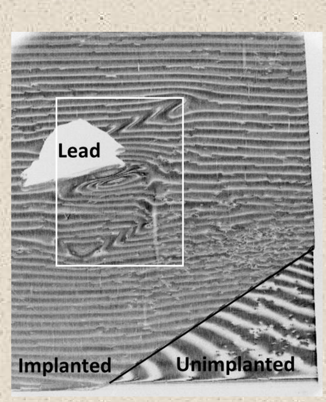

Topograph of sample 3

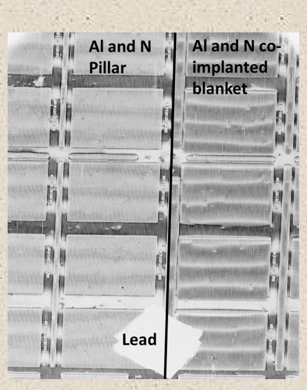

Topograph of sample 4

- Lead pieces were used as reference location
- nonuniformity of contours in white box is from the scratches
- Contours are narrower in the implanted samples, so the implantation create misorientation in the wafers.
- Contours are much narrower in sample 3 and 4, since implantation with Al could induce more damage

SRIM Damage Simulations

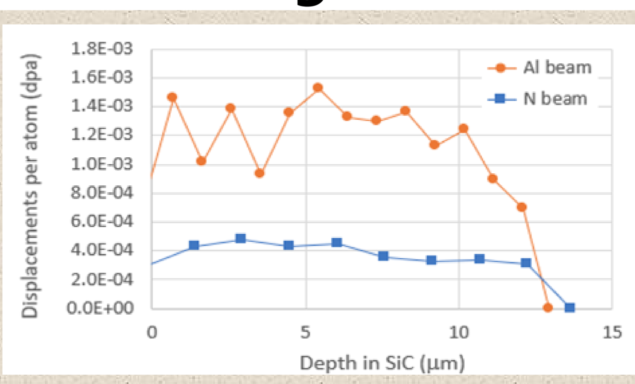

- Heavier dopant atoms have higher stopping energy, which is associated with formation of vacancies that could result in lattice strain
- A lower displacement per atom (dps) produced by nitrogen implantation leads to a lower extent of strain in sample 2

Reference

- [1] Tao Liu, et.al, IEEE Access, 145118 Volume 7,2019.
- [2] Nipoti, R, et.al, Materials Science Forum, 924, 333–338.
- [3] P. Thieberger, et.al, Nuclear Inst. and Methods in Physics Research B 442 (2019) 36–40

Strain Maps and Reciprocal Space maps (RSMs) of As-implanted Samples

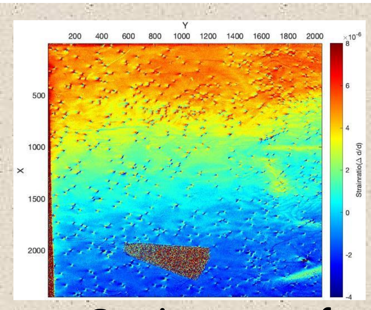

Strain map of sample 1

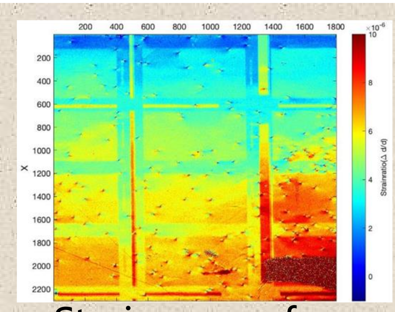

Strain map of sample 2

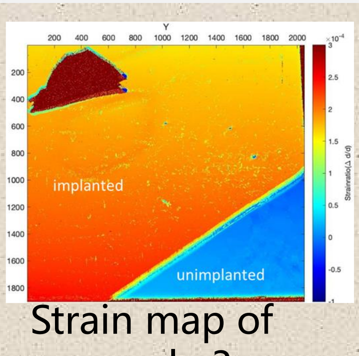

Strain map of sample 3

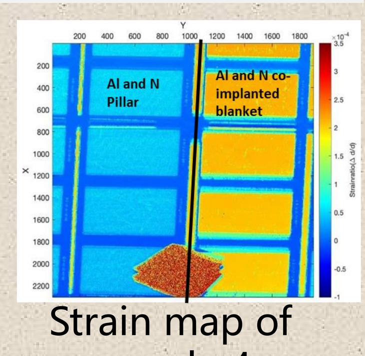

Strain map of sample 4

- Strain maps were derived from SXRCT data by Eq (1) and (2).
- The strain map of sample 1 and 2 illustrate a strain level of 10^{-6}. Strain level of implanted region of sample 3 is 1.5 to 2.5 x 10^{-4}, which is almost 20 times larger than that of sample 1. This result correlate with the damage simulation.
- Blanket pattern of sample 4 were co-implanted by Al and N, The actual fluence of blanket pattern is thus twice that of the pillar pattern. Based on the strain obtained from strain map, the strain level in blanket pattern is 2.8 times higher than in pillar pattern and correlates with fluence levels.

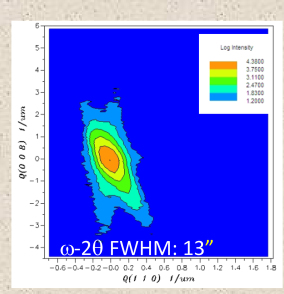

RSM of sample 1

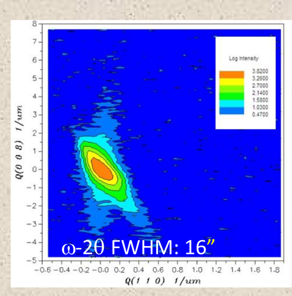

RSM of sample 2

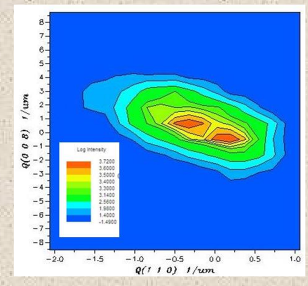

RSM of sample 3

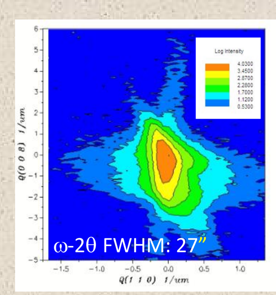

RSM of sample 4 pillar

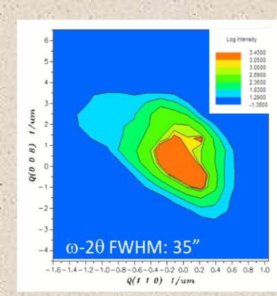

RSM of sample 4 blanket

- RSM of sample 2 revels low strain and Full width half max (FWHM) along ω-2ɵ axis is similar to that of sample 1. Significant strain exists in implanted region of sample 3 by showing an extra satellite peak in the RSM. The strain of sample 3 is higher than that of sample 2, since damages created by Al implantation is more significant.
- Due to difference in effective fluence, RSM of blanket pattern of sample 4 shows a broader peak than that of pillar pattern, meaning the extent of strain is more severe in blanket pattern.
- The results from RSMs correlate well with the results from strain maps and SRIM damage simulation.

Characterization of Post-annealed Sample

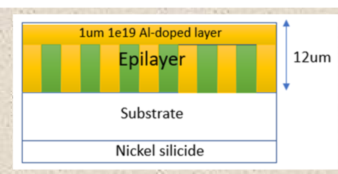

Super junction device structure

Sample	Dopant & concentration	Annealing condition	Implantation energy (max)	Comments
5	Al, 1e16 + N, 1e16, P+ Al	1700 °C / 60 min	65.7MeV	Super junction device
6	Al, 1e16 + N, 1e16, P+ Al	1800 °C / 60 min	65.7MeV	Super junction device
7	Al, 1e16 + N, 1e16, P+ Al	1900 °C / 60 min	65.7MeV	Super junction device
8	Al, 1e16 + N, 1e16, P+ Al	2000 °C / 60 min	65.7MeV	Super junction device

- Sample 5 to 8 are superjunction devices annealed at 1700 to 2000°C for 60 min

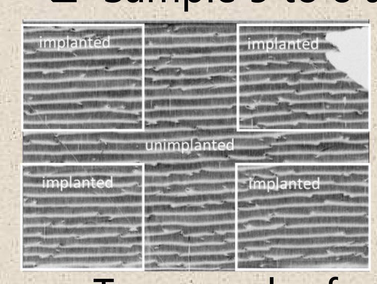

Topograph of sample 5

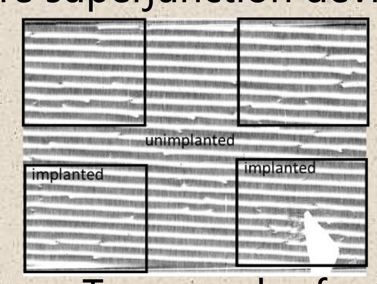

Topograph of sample 6

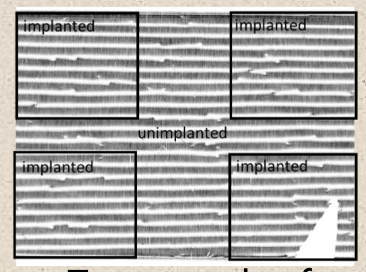

Topograph of sample 7

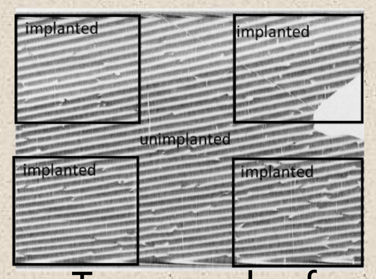

Topograph of sample 8

- Contours are uniform across implanted and unimplanted region for sample 5 to 8, indicating that the crystals have uniform strain.

Strain Maps and Reciprocal Space maps (RSMs) of Post-annealed Samples

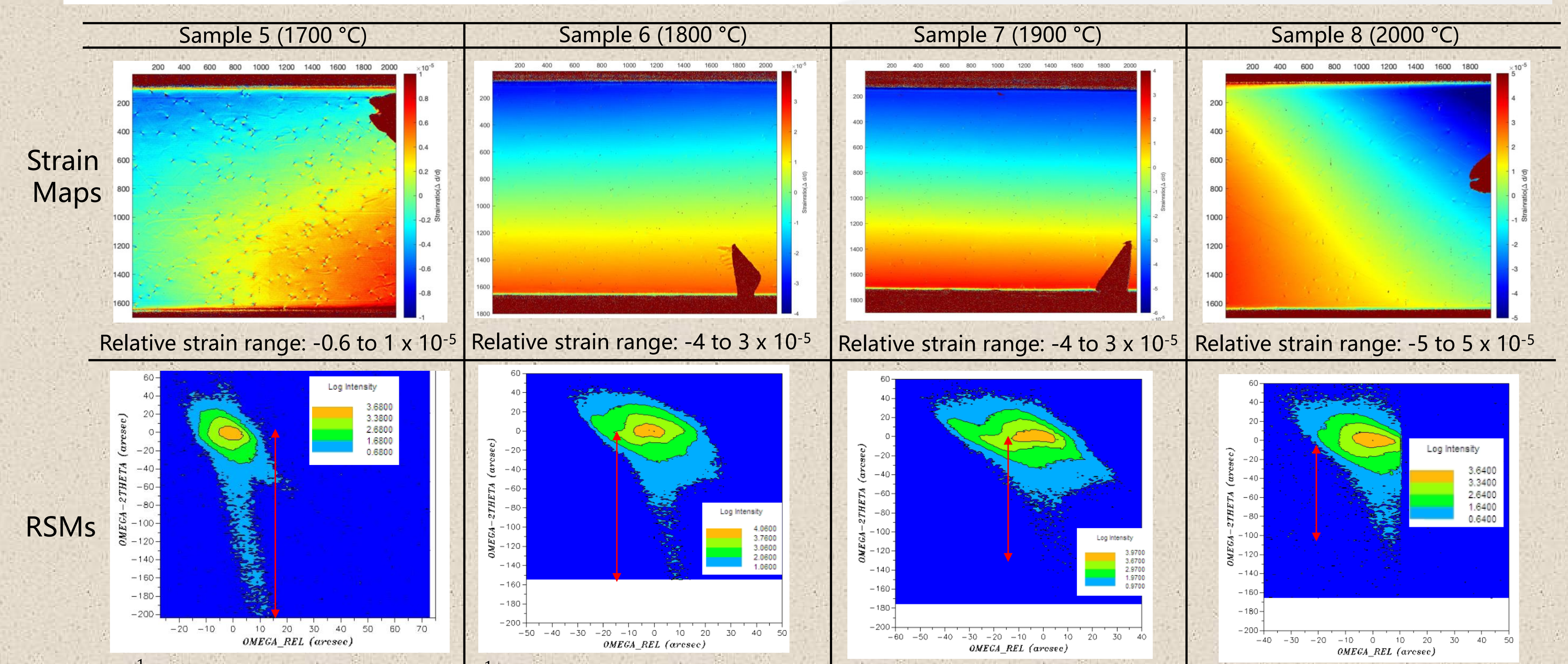

Relative strain range: -0.6 to 1 x 10^{-5} | Relative strain range: -4 to 3 x 10^{-5} | Relative strain range: -4 to 3 x 10^{-5} | Relative strain range: -5 to 5 x 10^{-5}

$\frac{1}{1000}$ of max intensity: -200 arc sec | $\frac{1}{1000}$ of max intensity: -140 arc sec | $\frac{1}{1000}$ of max intensity: -132 arc sec | $\frac{1}{1000}$ of max intensity: -130 arc sec

- Sample 5 to 8 have undergone annealing at 1700 to 2000C. the strain maps show recovery of major damage since strain in the samples are nearly uniform
- After the annealing process, some of the Si and C atoms may still remain displaced from the lattice site, resulting in residual tensile strain in the lattice
- Residual strain in the samples can cause a low intensity tail extending to the lower angular position along the omega 2 theta axis in the reciprocal space maps. We standardize the reciprocal space maps in $\frac{1}{2}$, $\frac{1}{10}$, $\frac{1}{100}$ and $\frac{1}{1000}$ intensity.
- There is a clear trend that the tail in reciprocal space map of sample annealed at higher temperature is shorter. Therefore, the residual strain is lower for sample annealed at higher temperatures. The mobility of the displaced atoms is higher at higher annealing temperatures and thus can move to the correct lattice site.

Acknowledgement

- The information, data, or work presented herein was funded in part by the Advanced Research Projects Agency-Energy (ARPA-E), U.S. Department of Energy, under Award Number DE-AR0001028. The views and opinions of authors expressed herein do not necessarily state or reflect those of the United States Government or any agency thereof.
- Samples provided by GE Research
- BNL Work supported by the U.S. Department of Energy, Office of Science, under Contract No. DE[1]SC0012704
- This research used resources of the Advanced Photon Source, a U.S. Department of Energy (DOE) Office of Science User Facility operated for the DOE Office of Science by Argonne National Laboratory under Contract No. DE-AC02-06CH11357. The Joint Photon Sciences Institute at SBU provided partial support for travel and subsistence for access to Advanced Photon Source.